Revista Mexicana de Astronomía y Astrofísica, **60**, 343–354 (2024)

https://doi.org/10.22201/ia.01851101p.2024.60.02.11

FEED-FORWARD NEURAL NETWORKS TO ESTIMATE STOKES PROFILES

Joan Manuel Raygoza-Romero[1], Irvin Hussein Lopez Nava[1], and Julio Cesar Ramírez-Vélez[2]

Received December 22 2023; accepted June 27 2024

ABSTRACT

Magnetic fields are believed to play a crucial role in stellar evolution. To better understand this evolution, it is essential to measure the magnetic fields on the stellar surface. These measurements can be achieved through spectropolarimetric observations, using the polarized radiative transfer equation. Magnetic field properties are inferred by adjusting the Stokes profiles. In this study, we propose a deep learning approach using a feed-forward neural network to estimate the Stokes profiles based on eight input parameters that describe the magnetic field configuration. To achieve this, we conducted scaling experiments on the data, explored different configurations of the FNN architecture, and compared two approaches. A model capable of accurately estimating the Stokes profiles I, Q and V was obtained. However, we encountered difficulties in estimating Stokes profiles Q and U when they have low amplitudes.

RESUMEN

Los campos magnéticos desempeñan un papel crucial en la evolución estelar. Para comprender mejor esta evolución, es esencial medirlos en la superficie estelar. Estas mediciones se logran mediante observaciones espectropolarimétricas, utilizando la ecuación de transferencia radiativa polarizada. Las propiedades del campo magnético se infieren ajustando los perfiles de Stokes. Este estudio propone un enfoque de aprendizaje profundo mediante una red neuronal *feed-forward* para estimar los perfiles de Stokes a partir de ocho parámetros que describen la configuración del campo magnético. Se realizaron experimentos de escalado, de diversas configuraciones de la arquitectura y se compararon dos enfoques. Se obtuvo un modelo que logra una estimación precisa de los perfiles de Stokes I, Q y V. Sin embargo, hubo dificultades para estimar los perfiles de Stokes Q y U cuando estos tienen una amplitud baja.

Key Words: methods: data analysis — polarization — stars: magnetic field

1. INTRODUCTION

Magnetic fields are the origin of solar and stellar activity, and it is widely accepted that they can play a very important role in stellar evolution: from young stars to compact objects. Furthermore, the strength and topology of the magnetic field vary depending on the evolutionary stage, i.e., the age of the star. Therefore, it is crucial to understand how stellar magnetic fields evolve (Ramírez-Vélez, J. C. et al. 2018).

Mapping and measuring stellar magnetic fields present several challenges due to the invisible nature of these fields and the complex interactions occurring within stars. However, over the years, different techniques and tools have been developed to address this task. One of the most used observational techniques is spectropolarimetry, which consists of obtaining simultaneously the intensity and the degree of polarization in spectral lines. This technique exploits the polarization state of the light emitted by a star to infer the presence and properties of the magnetic field. It is through the analysis of spectropolarimetric data that magnetic fields can be properly characterized (Degl'Innocenti & Landolfi 2006).

[1]Centro de Investigación Científica y Educación Superior de Ensenada (CICESE), Departamento de Ciencias de la Computación.
[2]Universidad Nacional Autónoma de México (UNAM), Instituto de Astronomía - Ensenada.

Therefore, the reliability of astronomical inferences largely depends on the accuracy of light measurements. In this sense, spectropolarimetry analyzes light based on its two fundamental characteristics: intensity and polarization degree (del Toro Iniesta 2003). The polarization of light is described through the Stokes profiles. These emerged from the mathematical theory of light polarization and were proposed in the 19th century by the British physicist George Gabriel Stokes. They consist of four numerical values that provide a complete description of the polarization state of light. These profiles are commonly identified as I, Q, U, and V. The profile I represents the intensity of the light, while the profiles Q and U represent linear polarization, and the profile V represents circular polarization. These profiles vary in response to the presence and properties of the magnetic field in the star.

To fit spectropolarimetric observations, theoretical codes are required. These codes solve the polarized radiative transfer equation (RTE) to synthesize the Stokes profiles from a given magnetic field configuration on the star. In this work, a generalized off-centered dipolar magnetic configuration will be considered, and atmospheric parameters such as effective temperature ($T_{\rm eff}$), rotational speed (v_r), gravity ($\log g$), among others, are fixed. To obtain synthetic spectra, the code COSSAM is employed (Stift 2000). Note that by using a dipolar configuration the magnetic field is not uniform over the surface. In our case, the star's surface is divided into 284 areas, and in each area, COSSAM calculates the so-called local Stokes profiles using the eight attributes that describe the magnetic geometry of the dipolar configuration. The local Stokes profiles are then integrated over the entire surface to obtain the resulting Stokes profiles that will be compared with the observations.

This process requires significant computational time for modeling. Using COSSAM implies a comprehensive theoretical approach based on RTE, and it also allows generating a broad data set. For this reason, in this work a deep learning-based model was developed to provide a reliable tool for synthesizing a large number of magnetic configurations for the Stokes profiles in an affordable manner.

2. RELATED WORK

Currently, studies on stellar magnetism are based on the analysis of Stokes profiles observed in stars. Through the RTE, it is theoretically possible to model different configurations of the stellar magnetic field. By fitting the observed profiles with those obtained using RTE, it becomes possible to recover the magnetic field configuration and/or atmospheric characteristics of the star. However, the process of fitting theoretically calculated Stokes profiles is computationally expensive (Gafeira et al. 2021), due to the time required by resolution methods to solve the differential equations of RTE to simulate a given magnetic model, specially if many spectral lines have to be considered simultaneously.

Faced with this challenge, the use of machine learning (ML) algorithms, particularly deep learning, has emerged as a possible solution. Initially, all the efforts were applied in studies of the solar magnetism: In the pioneer work in this field (Carroll & Staude 2001), the authors trained a multilayer perceptron (MLP) neural network to demonstrate the possibility to infer the magnetic and atmospheric model from a given set of Stokes profiles. Later, in Carroll & Kopf (2008), the authors used snapshots of magnetohydrodinamycs (MHD) simulations to produce synthetic Stokes profiles, which were used for training to study the depth stratification of the magnetic and atmospheric models and to identify magnetic flux tube structures.

In general, in the scientific literature, most of the ML models were focused on performing regressions of physical properties, or magnetic configuration, of the solar atmosphere (Asensio & Díaz 2019; Gafeira et al. 2021; Knyazeva et al. 2022). In these studies, local Stokes profiles were analyzed from a very small region of the solar disk, allowing for detailed spatial resolution. In contrast, some articles focused on stars beyond the Sun, and the Stokes profiles were obtained from the entire (integrated) disk, resulting in a lack of spatial resolution in these observations, as all stars were considered point sources in telescopes (Carroll et al. 2008; Ramírez-Vélez, J. C. et al. 2018; Córdova, J. P. et al. 2018).

In the stellar domain, two studies (Córdova, J. P. et al. 2018; Ramírez-Vélez, J. C. et al. 2018) employ a regressor model to predict the effective magnetic field of a star. The first one uses the mean Stokes V profile, whereas the other one also utilizes Stokes Q and U profiles. In the cited works, the Stokes profiles were used to train ML algorithms to use the model as regressor, and consequently, to infer the physical atmospheric properties (including the magnetic field). In this sense, and to our knowledge, only the work of Carroll et al. (2008) has focused on training a ML algorithm to obtain as output the Stokes profiles given a set of 5 free parameters of the atmospheric and magnetic model. Prior to the training, the authors applied a decomposition using principal component analysis (PCA) of the Stokes profiles, finding very

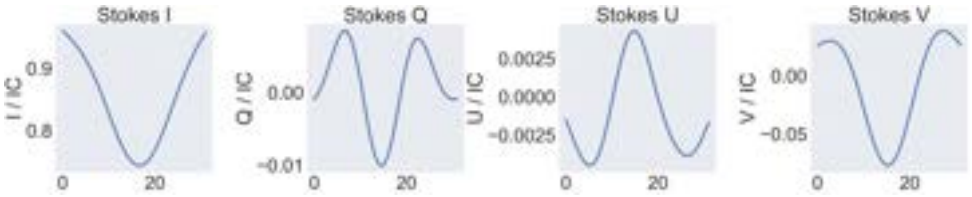

Fig. 1. Example of the four Stokes profiles. The color figure can be viewed online.

good results. The work we present here has a similar goal, to train a ML model to obtain the Stokes profiles given 8 free parameters of the magnetic configuration.

3. DATA SET

A synthetic data set generated by COSSAM was used to estimate Stokes profiles. Remembering that COSSAM employs the RTE to produce Stokes profiles (Stift 2000), a corpus of 1.3M data instances was generated in a spectral line at 6311.5 Å, with each instance having 8 attributes, namely the dipolar moment strength (m), the magnetic dipole position inside the star described by two coordinates (X_2, X_3), the rotation phase (p), three attributes describing the magnetic geometry of the dipolar configuration (α, β, γ), and the inclination angle (i) of the stellar rotation axis with respect to the line of sight. Each instance, with these eight input attributes, is associated with an output signal of 128 points, corresponding to the Stokes profiles, 32 points for each. Figure 1 shows an example of a signal generated with the following attribute values: $m = 1493.9, i = 35.7, \alpha = -58.4, \beta = 51.4, \gamma = -24.5, X_2 = 0.15, X_3 = 0.10, p = 0.64$; it was segmented into the four Stokes profiles that will be the output of our model.

This example highlights an important property in the Stokes profiles, which is the difference in amplitudes of each profile, with Stokes I being much larger than Stokes V, and Stokes V being larger than Stokes Q and U. Therefore, it is necessary to preprocess and scale the input and output data so that the prediction model will be able to estimate different magnitudes. Each instance was generated by selecting a random value from a uniform distribution for each input attribute ($m, i, \alpha, \beta, \gamma, X_2, X_3, p$) in the range shown in Table 1.

4. METHODS

The use of deep learning was motivated by the need to regress each point of the profile of each Stokes profile, thus requiring a multi-output model, and a feed-forward neural network (FNN) is suitable for this problem. In this study, two different metrics, namely the mean squared error (MSE) and the weighted mean absolute percentage error (WMAPE), were employed to evaluate the model's performance among several configurations. The following are the equations for each metric:

TABLE 1

RANGE FOR 8 INPUT ATTRIBUTES

Attribute	Min Value	Max Value
m	100.0	5010.0
X_2	0.00	0.20
X_3	0.00	0.20
p	0.0	1.0
α	-180.0	180.0
β	0.0	180.0
γ	-180.0	180.0
i	0.0	180.0

$$MSE = \frac{1}{n}\sum_{i=1}^{n}(Y_i - \hat{Y}_i)^2, \quad \text{and}$$
$$WMAPE = \frac{\sum_{i=1}^{n}|Y_i - \hat{Y}_i|}{\sum_{i=1}^{n}|Y_i|}, \tag{1}$$

where n is the number of points or sample, Y_i is the ground truth value, and $\hat{Y}_i$ is the model prediction for each point i.

MSE allows the comparison of different model configurations of the same data set. However, MSE penalizes larger errors more, as the differences between predicted and actual values are squared. On the other hand, WMAPE is a useful metric for comparing model predictions independently of the magnitude of the values being compared. As a percentage-based metric, WMAPE will be used to compare the accuracy of predicted values and true values between Stokes profiles. A good WMAPE is defined as being below 5%. It is important to emphasize that calculating the mean of this metric involves dividing the sum of WMAPE of each Stokes profile by the total number of Stokes profiles. This ensures that scale changes do not have a disproportionate impact and that all profiles are considered with equal weight.

Through the COSSAM code, combinations of values for the 8 attributes of the magnetic field (X_{cossam}) are provided, and in return, the four Stokes profiles (I, Q, U, V) denoted by (Y) are obtained. The FNN is responsible for estimating the Stokes profiles ($\hat{Y}$), and the error between Y and $\hat{Y}$ is calculated using the previously described metrics to evaluate the estimations. For all the work, the data set was split into 75% training, 15% validation, and 10% test, each of them having the same distribution among instances.

4.1. *Feed-forward Neural Network*

Feed-forward neural networks are a fundamental building block of deep learning architectures and have proven to be highly effective in many real-world applications (Paliwal & Kumar 2009). They consist of an input layer, one or more hidden layers, and an output layer, with the data flowing in a single direction from input to output. Each neuron in the network receives input from the previous layer, processes it using a set of weights and biases, and passes the result to the next layer. The hidden layers of the network are responsible for extracting complex features from the raw input data and transforming them into a representation suitable for the task at hand. The output layer provides the final prediction or decision.

The training of FNN is an optimization problem, where the objective is to find the set of weights and biases that minimize the prediction error on a training data set. This is typically achieved using an optimization algorithm, such as stochastic gradient descent or a variant thereof, and the back-propagation algorithm is used to compute the gradients of the error with respect to the weights and biases (Svozil et al. 1997).

4.2. *Selection of Neural Network Parameters*

The parameters for the following experiments are listed in Table 2. These parameters apply to all experiments, with some exceptions noted at the bottom of the table. In order to perform a wide range of experiments within a restricted timeframe, only a sample of the entire data set (50,000 instances) was considered.

These parameters were selected with some empirical experiments to determine them. The ReLU activation function was used in all layers except for the output layer, where no activation function was used. Based on the results of these preliminary experiments, a dynamic weight decay approach was applied. It consists of varying the weight decay as a function of the data set size, as weight decay plays a crucial role in the training process.

TABLE 2

FIXED PARAMETERS FOR FNN TRAINING

Attribute	Value
Data set Size	50,000
Momentum	0.95
Activation Function	ReLU
Epochs	1000
Optimizer	Stochastic gradient descent
Early Stopping	25
Learning Rate*	1
Batch Size	1024
Weight Decay	$1/(2 * dataset\_size)$
Loss Function	MSE

*Learning rates are variable in the scaling experiments.

This approach consists of varying the learning rate according to the number of epochs. A dynamic approach enables the adaptation of this parameter to the specific characteristics of the data set (Smith 2018). These neural network parameters are expected to enhance the overall effectiveness of the training process and improve the generalization capability of the network.

In this experiment, the Standard, Min-Max, Max-Abs and Quantile scalers were evaluated for both input (dipole moment strength, three Euler angles, inclination angle, two dipole position coordinates, and rotation phase) and output (32 points for each Stokes profile). This resulted in a total of 16 different models. As mentioned before, these models were trained and evaluated using a subset of the data, with the purpose of determining the optimal scaling method for both input and output of the model. The hyperparameters used in the FNN of this experiment were those listed in Table 2.

Figure 2 displays the results of combining different scaling methods using a baseline estimation model. Outliers were removed for improved analysis and visualization. On the X-axis, the scaling methods are grouped for the output scaler, while the color series correspond to the scaler on the input data.

4.3. *Scaling Selection*

In this visual representation, it is highlighted that the standard scaling method for output out-performs the others in terms of the mean WMAPE of all Stokes profiles (left of Figure 2). Regarding input scaling, no significant difference is observed among the different methods. However, to supplement this

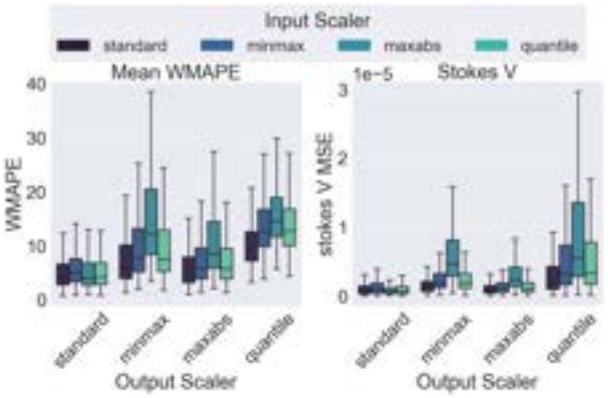

Fig. 2. Mean WMAPE of the Stokes profiles and the MSE of Stokes V for the different combinations of input and output scaling methods. The color figure can be viewed online.

information, the right graph in Figure 2 shows the MSE for the Stokes V, which is the most relevant profile in our research. Once again, a similar improvement is seen with the standard method for output. However, in the case of input scaling, a more noticeable difference is observed with the Max-Abs method.

By analyzing in detail each Stokes profile in Table 3, it can be noticed that the model using Max-Abs scaling for input along with standard scaling for output achieves better performance in terms of the MSE for each profile. Based on the results, it is recommended to select the Max-Abs scaling method for input and the standard scaling method for output.

4.4. *Architecture Selection*

A crucial aspect to consider is the choice of FNN architecture. Determining the optimal number of hidden layers and neurons per layer is essential for achieving the best performance. In our experiment, we tested different configurations, including 2, 3, 4, 5, 6, and 7 hidden layers with 512, 1024, 2048, and 4096 neurons per layer, resulting in a total of 24 models. This experiment was conducted using the input and output scaling previously selected (Max-Abs for input and standard for output).

In Figure 3, outlier data and results from the models with two layers are omitted to better visualize these outcomes. In the left side of Figure 3, the mean WMAPE of the Stokes profiles for these models is displayed, and it is evident that as we increase the number of hidden layers and the number of neurons per hidden layer, the model's performance improves. Furthermore, by looking at the right side of Figure 3, which presents the Stokes V MSE, we can see the same trend, with more improvement occur-

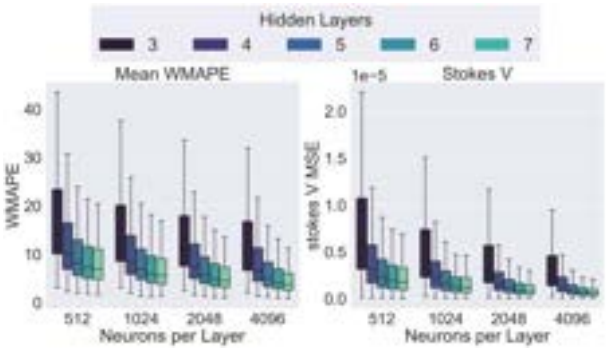

Fig. 3. Mean WMAPE of the Stokes profiles and the MSE of Stokes V for the different architectures of FNN grouped by the number of neurons per layer. The color figure can be viewed online.

ring with the number of hidden layers and neurons per layer.

In Table 4, the best-found architectures are presented. The largest model, with 7 hidden layers and 4096 neurons per hidden layer, scores lower MSE in each Stokes profile, as well as lower mean WMAPE. Based on the results of this experiment, the architecture with 7 hidden layers and 4096 neurons per hidden layer is selected. It is important to note that due to hardware limitations, experiments with more neurons and hidden layers cannot be conducted.

4.5. *General vs Specialized Models*

In the quest for the best model, we encountered two approaches. One of them involves creating a model to estimate each Stokes profile individually, resulting in a specialized model for each of them, named from now on "specialized models". On the other hand, we could employ a single model capable of predicting all four Stokes profiles simultaneously, i.e., a "general model". This leads us to the following question: Is it better to construct a specialized model for each Stokes profile or to use a single model capable of predicting all four profiles simultaneously?

In Figure 4 and Table 5, we present the results that showcase the comparative performance of these approaches. There is a notable difference between them, with the general model standing out in terms of performance. Both the general model and the specialized models contain the same input parameters, but somehow the general model benefits from containing the values of all Stokes profiles and therefore performs better than the specialized models in the experiments we performed.

In contrast, specialized models for each Stokes profile lack access to these values, as their aim is limited to predicting a specific profile. While these

TABLE 3

MEAN MSE PER STOKES PROFILE AND MEAN WMAPE OF THE STOKES PROFILES OF INPUT AND OUTPUT SCALING

Input Scaler	Output Scaler	S_I MSE	S_Q MSE	S_U MSE	S_V MSE	Mean WMAPE
Standard	Standard	1.2e-06	2.3e-07	1.6e-07	1.2e-06	**6.41**
Standard	Max-Abs	1.2e-05	2.4e-07	1.9e-07	1.2e-06	9.52
Max-Abs	Standard	**1.0e-06**	**1.7e-07**	**1.5e-07**	**1.0e-06**	8.33
Quantile	Standard	1.1e-06	2.1e-07	**1.5e-07**	1.1e-06	6.85

TABLE 4

MEAN MSE PER STOKES AND MEAN WMAPE OF THE STOKES BY NUMBER OF HIDDEN LAYERS AND NEURONS PER LAYER

Hidden Layers	Neurons	S_I MSE	S_Q MSE	S_U MSE	S_V MSE	Mean WMAPE
5	4096	1.3e-06	2.5e-07	2.1e-07	1.3e-06	11.03
6	4096	1.0e-06	1.7e-07	1.5e-07	1.0e-06	8.33
7	2048	1.2e-06	1.9e-07	1.5e-07	1.2e-06	8.39
7	4096	**9.3e-07**	**1.5e-07**	**1.2e-07**	**8.8e-07**	**7.09**

TABLE 5

MEAN MSE PER STOKES PROFILE AND MEAN WMAPE OF THE STOKES PROFILES FOR GENERAL AND SPECIALIZED MODELS

Model	S_I MSE	S_Q MSE	S_U MSE	S_V MSE	Mean WMAPE
Specialized	5.8e-06	4.4e-07	4.8e-07	1.5e-06	10.25
General	**9.3e-07**	**1.5e-07**	**1.2e-07**	**8.8e-07**	**7.09**

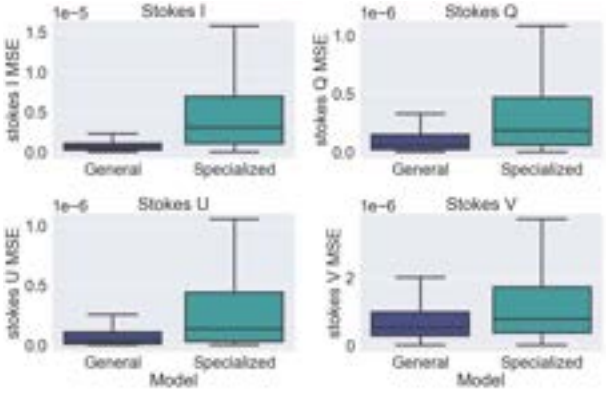

Fig. 4. MSE of each Stokes profile for general and specialized models. The color figure can be viewed online.

models can capture the unique characteristics of each individual Stokes profile; they cannot leverage the connections with neurons predicting the other Stokes profiles.

This limitation can lead to lower accuracy in predicting the Stokes profiles in isolation. As a result, the general model, by benefiting from the interaction among the Stokes profiles, out-performs the specialized models in terms of precision and predictive capability. These findings support the notion of using the general model to predict the Stokes profiles.

5. RESULTS

Based on previous experiments, we proceeded to evaluate the performance of the best model using the complete dataset (1.3M instances). In Table 6, we can observe the WMAPE for each Stokes profile as well as the mean WMAPE; along with the value for the third quartile as a measure of dispersion.

In summary, the model achieves good performance for Stokes I, Q, and V (lower than 2.79% of mean WMAPE), and a satisfactory performance for Stokes U (6.62%). The results demonstrate that the model is quite robust and reliable for all Stokes profiles.

TABLE 6

MEAN MSE PER STOKES PROFILE AND THE MEAN WMAPE OF THE STOKES PROFILES, ALONG WITH THE THIRD QUARTILE

S_I WMAPE (Q3)	S_Q WMAPE (Q3)	S_U WMAPE (Q3)	S_V WMAPE (Q3)	Mean WMAPE (Q3)
0.0279 (0.0348)	2.79 (2.35)	6.62 (4.76)	1.37 (1.59)	2.70 (2.13)

5.1. *Analysis of Error Based on Stokes profile Amplitude*

Next, a comprehensive analysis of WMAPE about the amplitude of the Stokes profile profile was conducted. However, before delving into the details, it is necessary to define the calculation of amplitude for each Stokes profile. The amplitude of the Stokes profiles is defined as follows:

$$Amplitude_{StokesI} = \min(Y_I), \tag{2}$$

$$Amplitude_{Stokes\lambda} = \max(\mid Y_\lambda \mid), \tag{3}$$

where Y_I is the Stokes I profile, λ is any Stokes profile of Q, U and V. Since the Stokes Q, U, and V profiles cross zero, the maximum value of absolute values belonging to the Stokes profile is taken.

Using these definitions of Stokes profile amplitudes, an analysis of error was conducted, as the amplitude changes in each profile. Bar graphs were generated, where each bar represents a range of amplitude. The height of the bar corresponds to the mean WMAPE of the test cases within that amplitude range, and a number is displayed above each bar representing the percentage of test cases found within that amplitude range. Additionally, vertical lines were plotted within each bar to represent the standard deviation.

In Figure 5, we observe the WMAPE of each Stokes profile across its amplitude range. The 100%, 94.1%, 90.3% and 97.2% of the data are shown for the Stokes profiles I, Q, U and V, respectively. This is in order to better visualize most of the instances. As the amplitude of Stokes I increases, we also observe an increase in the error.

In general, the amplitude of any of the Stokes profiles varies as function of the intensity of the magnetic field (the stronger the field, the larger the amplitude). In particular, for the case of Stokes I, this amplitude variation is not significant. Due to this, the FNN prediction of the Stokes I can be considered successful, since even in the worst cases, the WMAPE remains below 0.06%.

A smaller amplitude in the three polarized Stokes profiles (U, Q, V) signifies lower polarized light intensity, which is attributed to a weakly magnetized star or a large inclination angle of the star with respect to the line-of-sight (for Stokes V) or that the transverse component of the field is weak (for Stokes Q and U).

For the Stokes Q profile, it is found that as its amplitude decreases, the WMAPE increases. However, in 94.1% of the cases, the mean of WMAPE is less than 4.5%. This suggests that the model performs well to estimate the Stokes Q profile in the majority of cases.

The Stokes U profile also exhibits a similar trend to the Stokes Q profile. The WMAPE increases as the amplitude decreases. Additionally, it's noted that in 90.3% of the test data, the mean of WMAPE is less than 10%. Given that Stokes Q and U are linear polarizations, there is a notable difference in the predictive capability between Stokes Q and U, with the latter being slightly more challenging for the model to estimate. Nonetheless, in most cases, the model provides a good estimation of the Stokes U profile.

In order to explain why the FNN model reproduces the Stokes Q profiles better than the U profiles is necessary to compare their amplitudes.

We are using in COSSAM the de-centered dipolar model, in which the position of the dipole in the stellar interior is determined by two coordinates. Even if the use of two coordinates, instead of three, to determine the position of the dipole combined with the ranges of variation of the Eulerian and inclination angles is a general approach for all possible magnetic configurations (Stift 1975), it results in an imbalance in the amplitudes of the linear Stokes profiles: the amplitudes of the Stokes Q are greater than those of Stokes U. In consequence, the FNN model performs better for the Stokes Q profiles –with higher amplitudes– than for the Stokes U profiles. See the Appendix for a more details.

Finally, for the Stokes V profile, a situation similar to that of the Stokes Q and U profiles is observed. As the amplitude decreases, the WMPAE increases. However, it is found that in 97.2% of the test data, the WMAPE is below 2.6%, indicating that the model is quite robust in estimating it with a very low WMAPE.

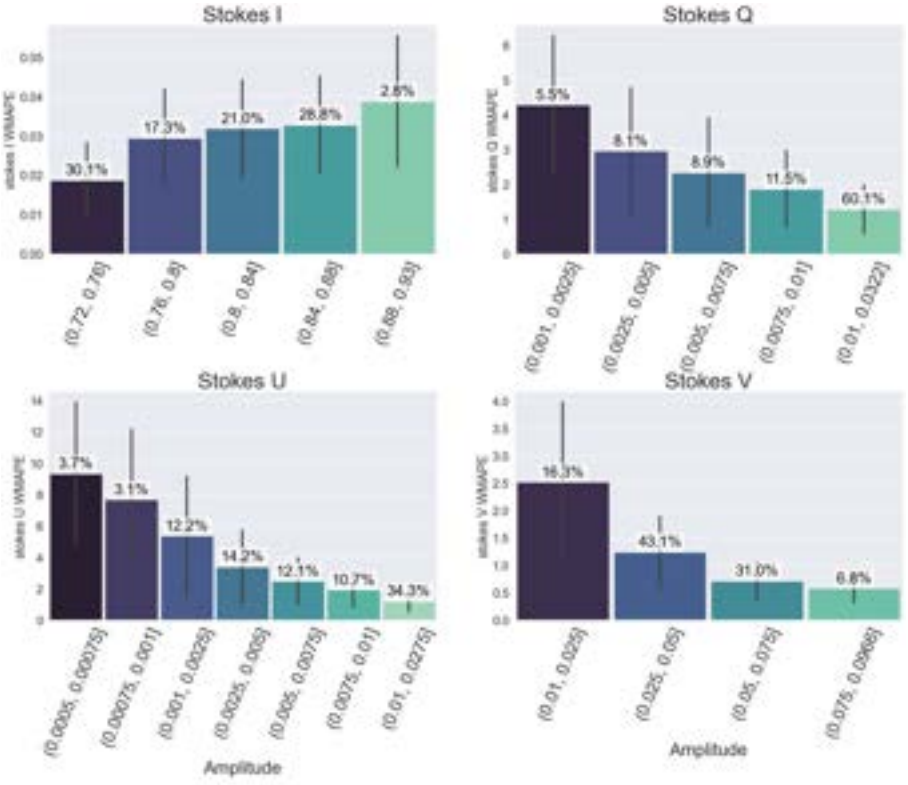

Fig. 5. WMAPE of each Stokes profile from the model for Stokes profile estimation grouped by amplitude ranges. The color figure can be viewed online.

5.2. *Percentile Analysis*

Finally, in Figure 6, we present the visualization of the 20th, 40th, 60th, 80th, 90th and 99th percentiles of the Stokes profile estimates based on the mean WMAPE of each Stokes profile. We can observe that in percentile 80th and below the model achieves a good performance in WMAPE on every Stokes profile. The results indicate that in 80% of cases the model performs well. At the 90th percentile, the mean WMAPE increases from 2.5% to 4.2%; the Stokes U profile proves to be the most challenging to estimate, with an error over 13%, but for the other Stokes profiles we obtain a good performance.

In the 99th percentile, representing one of the worst-case scenarios, the mean WMAPE is nearly 30%. The magnetic field configuration of this case has the following attribute values: $m = 127.4, i = 176.7, \alpha = 65.8, \beta = 57.1, \gamma = 156.5, X_2 = 0.139, X_3 = 0.057$ and $p = 0.70$. In this scenario, the Stokes U profile has an error of almost 70% (amplitude $\approx 5 \times 10^{-5}$), and the Stokes Q profile also exhibits a significant error, nearly 42% (amplitude $\approx 1 \times 10^{-4}$). Hence, in certain cases, the model does not respond adequately, specially if the amplitudes of the linear Stokes profiles are very low. Nonetheless, the Stokes V profile has an error of 7.1%, indicating that even in the worst cases, the estimation of the Stokes V profile remains with acceptable performance. Across all cases, the Stokes I profile is consistently well estimated by the model. We then conclude that in those magnetic configurations which produces a low amplitude of the Stokes profiles Q and U, the model has difficulties in their estimation, while for V and I Stokes profiles the performance of the model is quite acceptable for all magnetic configurations.

6. CONCLUSION AND FUTURE WORK

Through our research, deep learning models were implemented and evaluated to estimate Stokes profiles. We employed a feed-forward neural network due to its multi-output capability and adaptability to the problem. Additionally, experiments were conducted to determine the appropriate FNN architecture. The obtained results were highly satisfactory. When estimating Stokes profiles I and V, we

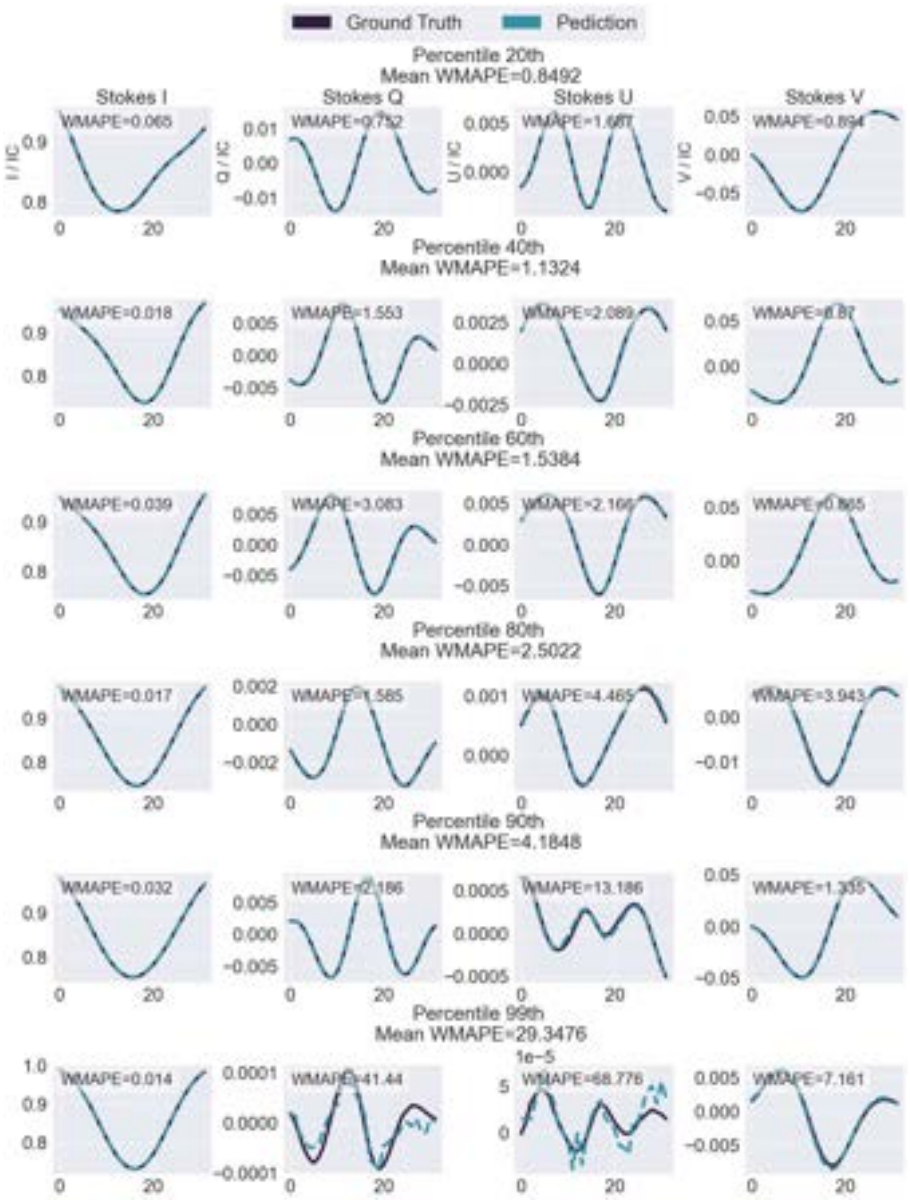

Fig. 6. Estimation of the Stokes profiles for the 20th, 40th, 60th, 80th, 90th and 99th percentile. The color figure can be viewed online.

achieved an MSE of 1.0e-07 and 9.1e-08, respectively. In terms of WMAPE, we obtained 0.02% and 1.37% for Stokes profiles I and V.

However, for Stokes profiles Q and U, the model struggled to accurately estimate these two Stokes profiles, obtaining 2.79% and 6.62% of WMAPE respectively. Our findings reveal a correlation between the amplitude of the Stokes profiles and the corresponding estimation errors. Specifically, as the amplitude decreases, the errors exhibit an upward trend. Notably, the estimation is better for Stokes I, followed sequentially by Stokes V, Q, and U, mirroring the decreasing amplitude order of these profiles. In some cases where the Stokes amplitudes Q and U are very small, we find that the model has difficulties in estimating them.

A potential avenue for future research involves utilizing the trained model to conduct inversions. This process entails optimizing the input attributes to adjust an observed Stokes profile to a synthesized profile generated by the model, with the ultimate goal of recovering the magnetic configuration of a

star and applying the developed methodology to real data obtained from astronomical observations. In this sense, our goal is to use the trained FNN to analyze the observed Stokes profiles and consequently recover the magnetic field configuration of real stars.

It is important to emphasize that this study does not consider noise of the Stokes profiles, but evaluating its impact on model performance is crucial. This strategy would simulate more realistic situations, as astronomical data in practice often contain noise.

Furthermore, it is interesting to experiment with other architectures of deep neural networks, such as recurrent networks, convolutional networks, or transformers. These architectures could offer additional advantages in terms of capturing temporal patterns, extracting spatial features, or modeling long-range relationships. Exploring these alternatives could provide new insights and further enhance the model performance.

Finally, the model presented here can be used as a basis for training other neuronal models through the so-called *transfer technique* (Zhuang et al. 2021). This approach has the great advantage for training new neuronal models with fewer instances, since a pre-trained model for a similar task is used. In other words, we can use the presented model for training other models dedicated to the synthesis of polarized spectral lines at different wavelengths, or the synthesis of multi-line profiles as the LSD profiles with fewer data in a shorter time and with a similar performance.

This work is funded by the Mexican National Council for Science and Technology (CONACYT), under Grant number 806073. We would like to thank the UNAM- PAPIIT Grant IN118023.

APPENDIX

In Figure 7 we show from top to bottom the distribution of the amplitudes of Stokes Q, U and V profiles using the dipolar de-centred approach. The left column corresponds to the training sample (1.3 million instances), while in the right column, and for consistence purposes, are included the amplitudes of another spectral line, namely Fe at 4503 Å for a smaller sample of 50,000 instances.

We remark that the distributions of both columns follow a similar tendency, where the amplitudes of Stokes V are the largest (as they should be), while the amplitudes of the Stokes Q are larger than those of Stokes U. As we mention, this is due to the fact that in COSSAM the position of the dipole is given by two coordinates instead of three, inducing an amplitude difference in the lines Stokes profiles. This in turn is the reason why the FNN perform better for Stokes Q than for Stokes U profiles.

Finally, in Figure 8 we show the same as in Figure 7 but for the centered dipolar model. In this case we can notice that the amplitudes of the linear Stokes profiles cover the same ranges; it should be expected that the FNN could perform equally well for both, Stokes Q and Stokes U.

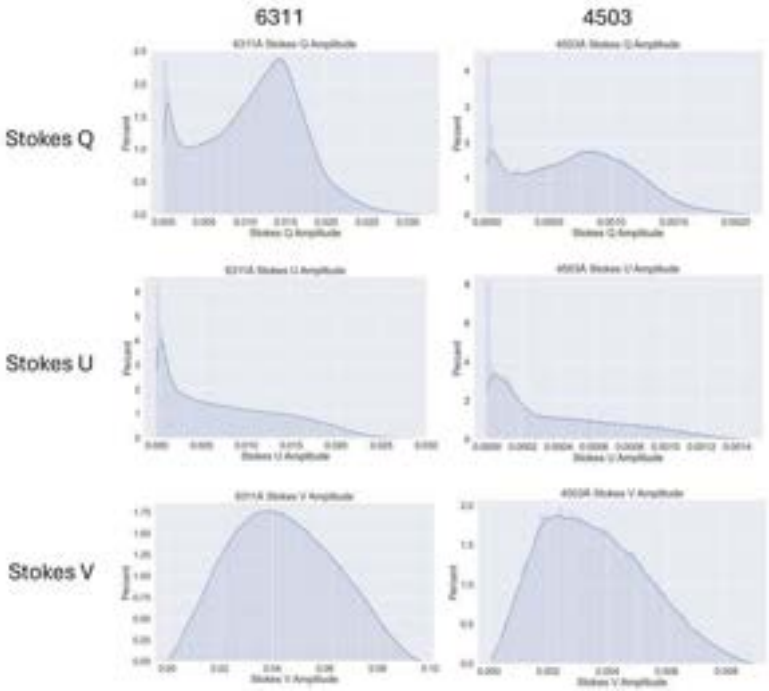

Fig. 7. Percent distribution of amplitudes of the polarized Stokes parameters. The left column corresponds to the total sample used for training (1.3 M instances), while the right column corresponds to the Fe line at 4503 Å (sample of 50 k instances). The color figure can be viewed online.

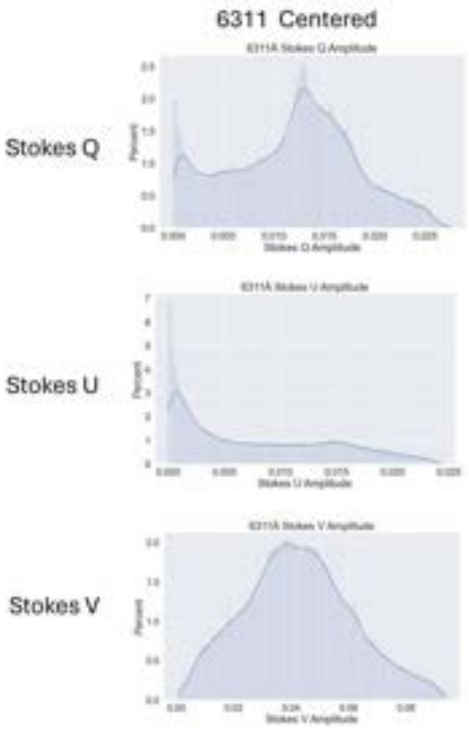

Fig. 8. Similar to Figure 7 but for a centered dipolar model (the dipole is in the center of the star). The amplitudes correspond to a sample of 50,000 instances for the Fe 6311 Å line. In this case, the amplitudes of the linear Stokes profiles cover the same range of amplitudes. The color figure can be viewed online.

REFERENCES

Asensio, A. & Díaz, C. J. 2019, A&A, 626, 102, https://doi.org/10.1051/0004-6361/201935628

Carroll, T. A. & Kopf, M. 2008, A&A, 481, 37, https://doi.org/10.1051/0004-6361:20079197

Carroll, T. A., Kopf, M., & Strassmeier, K. G. 2008, A&A, 488, 781, https://doi.org/10.1051/0004-6361:200809981

Carroll, T. A. & Staude, J. 2001, A&A, 378, 316, https://doi.org/10.1051/0004-6361:20011167

Córdova, J. P., Navarro, S. G., & Ramírez-Vélez, J. C. 2018, International Journal of Computational Intelligence Systems, 11, 608, https://doi.org/10.2991/ijcis.11.1.46

Degl'Innocenti, M. L. & Landolfi, M. 2006, Polarization in spectral lines, Vol. 307 (Springer Science & Business Media), https://doi.org/10.1007/1-4020-2415-0

del Toro Iniesta, J. C. 2003, Introduction to spectropolarimetry (CUP), https://doi.org/10.1017/CBO9780511536250

Gafeira, R., Orozco, D., Milić, I., et al. 2021, A&A, 651, 31, https://doi.org/10.1051/0004-6361/201936910

Knyazeva, I., Plotnikov, A., Medvedeva, T., & Makarenko, N. in Advances in Neural Computation, Machine Learning, and Cognitive Research V, 2021, ed. B. Kryzhanovsky, W. Dunin-Barkowski, V. Redko, Y. Tiumentsev, and V. V. Klimov, 299, Springer, Cham, https://doi.org/10.1007/978-3-030-91581-0_40

Paliwal, M. & Kumar, U. A. 2009, Expert systems with applications, 36, 2, https://doi.org/10.1016/j.eswa.2007.10.005

Ramírez-Vélez, J. C., Yáñez, C., & Córdova, J. P. 2018, A&A, 619, 22, https://doi.org/10.1051/0004-6361/201833016

Smith, L. N. 2018, arXiv:1803.09820, https://doi.org/10.48550/arXiv.1803.09820

Stift, M. J. 1975, MNRAS, 172, 133, https://doi.org/10.1093/mnras/172.1.133

Stift, M. J. & Leone, F. 2003, A&A, 388, 411, https://doi.org/10.1051/0004-6361:20021605

Svozil, D., Kvasnicka, V., & Pospichal, J. 1997, Chemometrics and Intelligent Laboratory Systems, 39, 43, https://doi.org/10.1016/S0169-7439(97)00061-0

Zhuang, F., Qi, Z., Duan, K., et al. 2021, Proceedings of the IEEE, 109, 43, https://doi.org/10.1109/JPROC.2020.3004555

Irvin Hussein Lopez Nava and Joan Manuel Raygoza-Romero: Ciencias de la Computación, Centro de Investigación Científica y de Educación Superior de Ensenada, Carr. Tijuana-Ensenada km107, 22860 Ensenada, Baja California, México (jraygoza, hussein@cicese.edu.mx).

Julio Cesar Ramírez-Vélez: Instituto de Astronomía, Universidad Nacional Autónoma de México, Carr. Tijuana-Ensenada km107, 22860 Ensenada, Baja California, México (jramirez@astro.unam.mx).